

PAPER • OPEN ACCESS

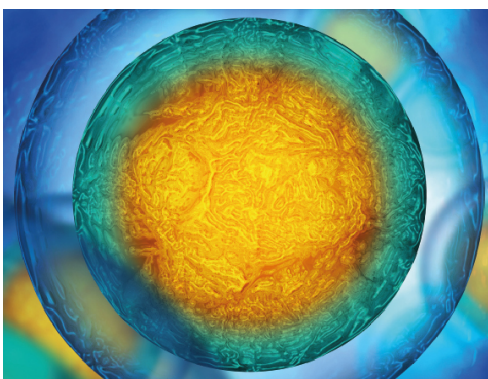
## Characterization of a customized 3D-printed cell culture system using clear, translucent acrylate that enables optical online monitoring

To cite this article: Ina Gerhild Siller *et al* 2020 *Biomed. Mater.* **15** 055007

View the [article online](#) for updates and enhancements.

### Recent citations

- [Steffen Winkler \*et al\*](#)
- [Miniaturized freeflow electrophoresis: production, optimization, and application using 3D printing technology](#)  
JohnAlexander Preuss *et al*
- [Customizable 3D-Printed \(Co-\)Cultivation Systems for In Vitro Study of Angiogenesis](#)  
Ina G. Siller *et al*



IOP | ebooks™

Your publishing choice in all areas of biophysics research.

Start exploring the collection—download the first chapter of every title for free.

# Biomedical Materials



## PAPER

### OPEN ACCESS

RECEIVED  
3 February 2020

REVISED  
31 March 2020

ACCEPTED FOR PUBLICATION  
29 April 2020


PUBLISHED  
16 July 2020

Original content from this work may be used under the terms of the [Creative Commons Attribution 4.0 licence](#).

Any further distribution of this work must maintain attribution to the author(s) and the title of the work, journal citation and DOI.



# Characterization of a customized 3D-printed cell culture system using clear, translucent acrylate that enables optical online monitoring

Ina Gerhild Siller , Anton Enders, Pia Gellermann, Steffen Winkler, Antonina Lavrentieva, Thomas Scheper and Janina Bahnemann

Institute of Technical Chemistry, Leibniz University Hannover, Callinstraße 5, Hannover 30167, Germany

E-mail: [jbahnemann@iftc.uni-hannover.de](mailto:jbahnemann@iftc.uni-hannover.de)

**Keywords:** 3D printing, additive manufacturing, biocompatibility, mammalian cell culture, biomaterials, rapid prototyping

Supplementary material for this article is available [online](#)

## Abstract

Cells are very sensitive to their direct environment—they place high demands, for example, on ambient culture medium, adjacent cell types, and the properties of surrounding material parts. As a result, mechanical and physical material properties—such as surface roughness, swelling, electrostatic effects, etc—can all have a significant impact on cell behaviour. In addition, a material's composition also impacts whether that material meets biocompatibility requirements and can thus be considered for potential use in biomedical applications. The entry of high-resolution 3D printing technology in biotechnology has opened the door to individually-designed experiment-adaptable devices of almost unlimited complexity that can be manufactured within just a few hours. 3D printing materials are frequently lacking in the characteristics that make them suitable for biomedical applications, however.

This study introduces a high-resolution polyacrylic 3D printing material as a potential alternative material for use in cultivation systems with indirect or direct contact to cells. Viability analyses, studies of apoptotic/necrotic cell death response, and surface studies all suggest that this material meets the requirements for (*in vitro*) biocompatibility, and has surface properties sufficient to permit uninhibited cell proliferation for cells in direct contact to the material. Moreover, the translucency of this material facilitates the type of optical monitoring required for performing experiments in a microfluidic environment, or for facilitating microscopic observations.

## 1. Introduction

In 1983, the US American engineer Charles 'Chuck' Hull came up with the idea of the first 3D printing apparatus, which was capable of creating objects in a layer-by-layer fashion [1]. Shortly thereafter, he filed a patent for his revolutionary idea. 3D printing (also known as additive manufacturing) has since transformed traditional manufacturing, enabling the fabrication of individually designed complex systems in an astonishingly short amount of time. After Hull's initial patents expired, 3D printing technology quickly became widespread across a variety of industries and disciplines. 3D printing technology also

soon found its way into scientific applications, and it is now established in the medical sector, where it facilitates modern-day 'miracles' including complex surgical models and customized patient-specific prostheses based upon medical imaging data [2, 3]. In the wet lab environment, 3D printing has turned out to be a valuable tool for creating experiment-specific labware and individually adjusted prototypes ('rapid prototyping') [4, 5]. And with more recent developments in advanced 3D printers that permit printing in high resolution of under 100  $\mu\text{m}$ , this technology has also found important applications in microfluidics and biomedical engineering [6–8]. In microfluidics, high-definition 3D printing technology now

allows researchers to manufacture 3D geometries with almost unlimited complexity in virtually no time.

As diverse as these applications are, so are the underlying 3D printing technologies that have been developed. The material bases can vary from photosensitive liquid acrylates (which are cured via photopolymerization) to rigid thermoplastic materials (which are fused and extruded in strands) to powdered material particles (which are selectively sintered with a laser)—to give just a few illustrative examples. Regardless of their differences, however, all 3D printing technologies have one thing in common: they utilize a ‘layer-by-layer’ fabrication process. In this study, objects were printed via inkjet 3D printing technology. The printer uses ultraviolet (UV) light curable material in liquid form that is ejected from the inkjet head as it moves forward. During the subsequent backward movement, the material is flattened by a roller and cured via a UV lamp. This process is then repeated, layer-by-layer, until the desired object is fully built up.

For integration of 3D-printed objects into biomedical applications, the biological environment needs to be in compliance with specific material properties. Whenever a biological system (such as a cell) is brought into direct contact with a material, interface interactions can transpire. Properties of the material can provoke changes in the biological environment—which can in turn have an additional effect on the material, etc, creating a feedback loop effect. As a result, the chemical, mechanical, and physical properties of a material are all critical factors that can each potentially limit the incorporation of that material into biological applications. Aside from consideration of the general non-toxicity of a material, however, two surface characteristics have been identified in the literature as having critical parameters for influencing cellular behaviour: wettability, and surface topography/roughness [9–11]. Surface wettability plays a major role in cell attachment and growth, because it can impact protein adsorption. Cell attachment is regulated via proteins—giving one reason for using serum-enriched cell culture medium, which is containing these specific proteins [9]. The proteins adsorb onto the materials surface, and then provide binding sites for cell anchorage. Surface topography at both micro- and nano-scales also has implicated for cell adhesion and proliferation. After studying surface wettability and topography independently, Yang *et al* have shown the dependency of osteoblast adhesion and spreading on surface roughness of polystyrene films [10]. But other material properties can also potentially affect the surrounding biological environment: these include (to name just a few) material tensile strength, flexibility, hardness, durability, surface charge, and energy or electrostatics [12]. To overcome potential adverse material properties of 3D printing resins, Lu *et al* have illustrated the

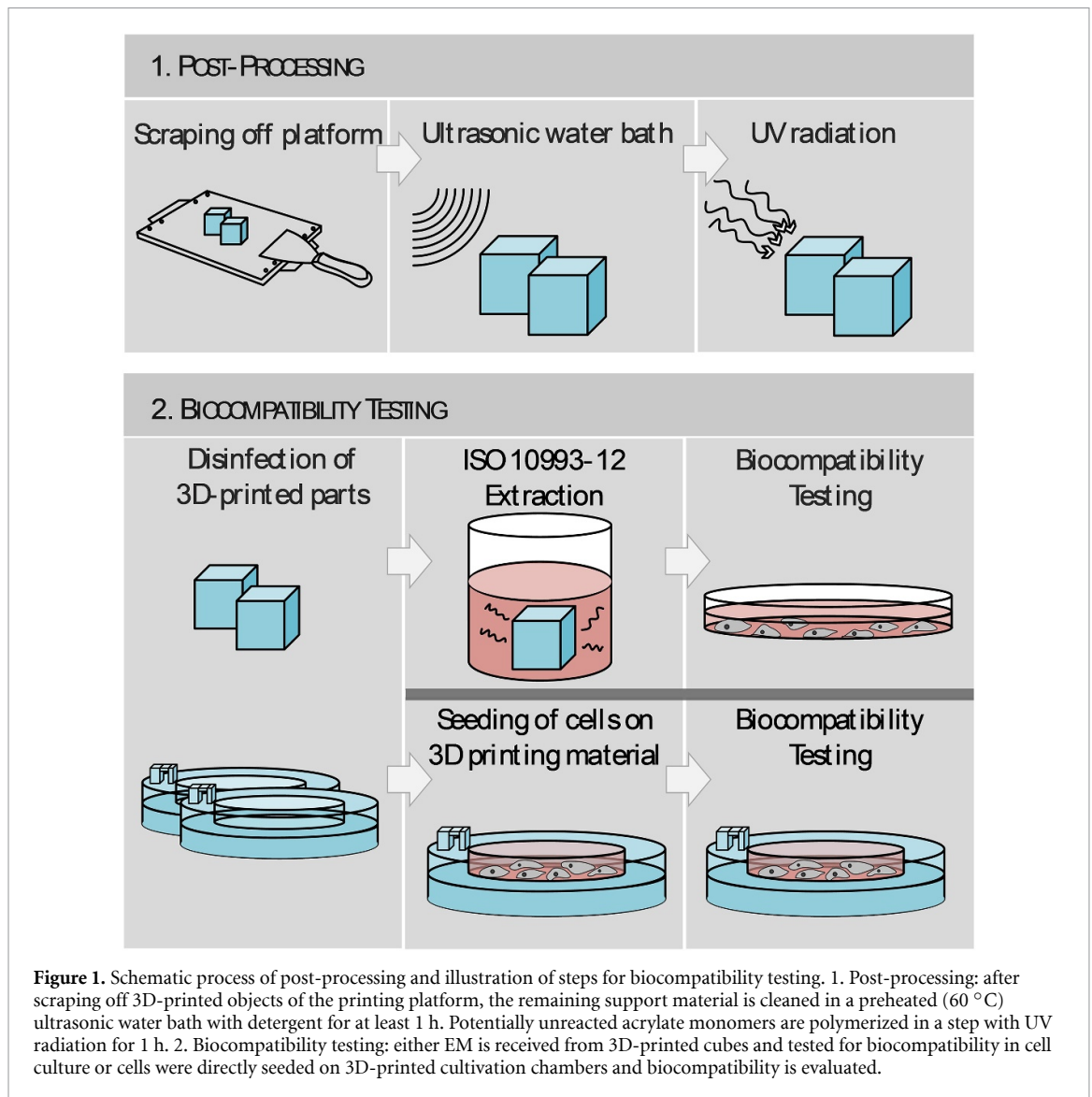
effectiveness of using waterborne polyurethane as a coating material [13]. This improved both cell adhesion and proliferation compared to uncoated material. It should be apparent that there are many factors to consider in this equation. But even if all mechanical, physical, and physico-chemical properties of a material meet the desired requirements, enhanced cytotoxicity may *still* disqualify the material for any biological studies. Put differently (and simply): in order to qualify for use in biological studies, it must be shown that a material has no negative influence on cell growth and proliferation compared to certified cell culture materials. The biocompatibility of a material must be established within restrictions or limitations.

Against this backdrop, then, this work represents a comprehensive investigation of a rigid, clear 3D-printed acrylic resin for potential use in biological applications and highlights the application in adherent cell culture by designing and characterizing a customized 3D-printed cell culture system. This study not only demonstrates the applicability of the 3D printing material in countless biological fields with regard to biocompatibility, but also emphasizes its suitability for the cultivation of adherent growing cells. Due to the printing process used, different surface topographies are formed. Depending on the desired application, the surface structure may have an impact. For that reason, the surface roughness and 3D profile of structures formed by the 3D printing process were analysed. And the potential influence of ethanol on these surface properties was also investigated—since ethanol is commonly used for disinfection of the 3D-printed objects. As mentioned above, biocompatibility is a central and prerequisite requirement for the use of any material in biological applications. The 3D printing material used in this study has not yet been certified as biocompatible, and to the best of our knowledge, there are no studies published yet that integrate additive manufactured systems into biological applications printed with this material. Accordingly, in order to evaluate as a matter of first impression the biocompatibility of this material, standard viability analyses based on biochemical assays as well as flow cytometric studies of apoptotic and necrotic cell responses were conducted. A customized cell culture system for adherent cell cultivation was designed, 3D-printed and examined for its suitability in biomedical applications. Since translucency of the 3D-printed material allows for optical observations, morphological changes in response to direct cell-material contact could be monitored by microscopic experiments.

## 2. Methods

### 2.1. 3D printing and post-processing

The analysed objects, cubes, and co-cultivation chambers were constructed with the computer-aided design (CAD) software SolidWorks 2018 (Dassault



Systèmes, Waltham, MA, USA). The printing material analysed in this study is named AR-M2 (Keyence Deutschland GmbH, Neu-Isenburg, Germany), and it is a rigid translucent polyacrylate resin printed using the high-resolution 3D printer AGILISTA-3200 W (Keyence Deutschland GmbH, Neu-Isenburg, Germany). Via a UV curing process, and using inkjet printing technology, a layer thickness of 15  $\mu\text{m}$  and a resolution of  $635 \times 400$  dots per inch can be achieved. The material appears as stable and translucently clear, enabling optical microscopic analyses. The known material components in a liquid state of the polyacrylate are two acrylate monomers, a photoinitiator, a stabiliser, and a urethane-acrylate-oligomer. AR-S1 (Keyence Deutschland GmbH, Neu-Isenburg, Germany) was used as support material during the printing process.

The support material is removed via several additional post-processing steps (figure 1). After roughly scraping the 3D-printed objects off the printing platform, remaining support material is removed by placing the objects for at least 1 h in a pre-warmed

(60 °C) ultrasonic water bath (Banedlin electronic, Berlin, Germany) with detergent (Fairy Ultra Plus, Procter and Gamble, CT, USA). This water bath is filled with deionized water provided by Arium® (Sartorius Stedim Biotech GmbH, Göttingen, Germany). To ensure proper photo polymerization of the materials acrylate monomers, the 3D-printed objects are additionally exposed to UV light (UV Sterilization Cabinet KT-09DC, Alexnld, Tiberias, Israel) for 1 h.

Since the 3D-printed material deforms at temperatures around 80 °C, thermal sterilization approaches are not applicable here [14, 15]. Instead, a chemical disinfection procedure with ethanol was used in this study. The 3D-printed objects were immersed for 1 h in ethanol (Carl Roth GmbH und Co. KG, Karlsruhe, Germany), 70%, v/v, placed for at least 30 min in a sterile environment (safety bench hood cabinet) allowing residues of ethanol to evaporate and washed thoroughly with sterile phosphate-buffered saline (PBS, Carl Roth GmbH und Co. KG, Karlsruhe, Germany) afterwards.

## 2.2. Chemical stability testing and surface analysis

To determine chemical stability,  $5 \times 5 \times 5$  mm cubes with a total surface area-to-volume-ratio of  $1.5 \text{ cm}^2 \cdot \text{ml}^{-1}$  were 3D-printed, post-processed, and incubated for 1 h, 24 h, 7 d and 14 d, respectively, in three different chemical solvents at RT. Isopropyl alcohol (70%, v/v) and ethanol (70%, v/v) were selected as chemical solvents since they are all commonly used in disinfection approaches for cell culture applications. Both before and after incubation, the 3D objects were dried (70 °C, 60 min), weighed, and subjected to surface studies (i.e. roughness, etc). The mass difference was then calculated, and both the color and the roughness parameters were observed using a digital microscope (VHX-5000, Keyence Corp., Osaka, Japan).

## 2.3. Preparation of extraction media for biocompatibility studies

To evaluate the biocompatibility of the aforementioned material, extraction medium (EM) is obtained according to EN ISO 10993-12:2012 (Biological evaluation of medical devices—art 12: Sample preparation and reference materials).  $5 \times 5 \times 5$  mm cubes with a total surface area of  $1.5 \text{ cm}^2$  were 3D-printed, post-processed, disinfected with ethanol (70%, v/v), and incubated in a cell culture medium (Minimum Essential Medium Eagle, with alpha modification ( $\alpha$ -MEM) (Thermo Fisher Scientific Inc. Waltham, USA), 10% human serum (c.c.pro GmbH, Oberdorla, Germany), and 0.5% Gentamicin (PAA Laboratories GmbH, Pasching, Austria)). The 3D-printed cubes were incubated in cell culture medium for 72 h at 37 °C in a 5% CO<sub>2</sub>, 21% O<sub>2</sub>, humidified atmosphere (Heracell 150i incubator, Thermo Fisher Scientific Inc. Waltham, USA) with a surface area/volume ratio of  $3 \text{ cm}^2 \cdot \text{ml}^{-1}$ . The obtained medium is referred to as EM. As a control, cell culture medium was also incubated for 72 h at 37 °C in a 5% CO<sub>2</sub>, 21% O<sub>2</sub>, humidified atmosphere in the absence of any 3D-printed cubes.

## 2.4. Cell line and cell culture conditions

In this study, experiments with human adipose tissue-derived mesenchymal stem/stromal cells (AD-MSCs) were performed. Following isolation from adipose tissue after abdominoplasty surgery, these cells were expanded and cryopreserved in passage 2 until used for biocompatibility studies. The donor has given informed written consent as approved by the Institutional Review Board (Hannover Medical School) with the reference number 3475–2017. The isolated cells have been previously extensively characterized as AD-MSCs [16]. AD-MSCs were cultivated in cell culture medium (described in 2.3.) at 37 °C in a 5% CO<sub>2</sub>, 21% O<sub>2</sub>, humidified atmosphere and harvested at about 85% confluency by accutase treatment (Merck KGaA, Darmstadt, Germany). All experiments were performed with cells of passages three to nine. Cell

proliferation was also monitored, and images were taken, via live cell imaging microscopy in the cell imaging multi-mode reader Cytation-5 (BioTek Instruments, Inc. Winooski, VT, USA).

## 2.5. CellTiter-Blue® viability assay

To evaluate cell viability, CellTiter-Blue® (CTB) cell viability assay (Promega, GmbH, Mannheim, Germany) was performed as instructed by the manual, including background and standard controls. Viable cells possess the ability to convert an indicator dye, the blue resazurin, into a purple, fluorescent product (resorufin) [17, 18]. Metabolically inactive cells are not able to reduce resazurin, and, as a result, they do not produce any fluorescent signal. Therefore, the detection of fluorescence intensity gives an indication on cell viability in the sample.

The fluorescent product formation is monitored at an extinction wavelength of 544 nm, and an emission wavelength of 590 nm, using a fluorescence plate reader (Fluoroskan Acent, Thermo Fisher Scientific Inc. Waltham, USA). Cells were seeded in 96-well plates (Sarstedt AG & Co. KG, Nürnbrecht, Germany) (at a density of  $1100 \text{ cells} \cdot \text{cm}^{-2}$ ) 24 h prior to the start of an experiment, and thereafter maintained at 37 °C in a 5% CO<sub>2</sub>, 21% O<sub>2</sub>, humidified atmosphere. The cell culture medium is exchanged to EM or control medium for another cultivation period of 24 h. After 24 h, the medium was removed from each well, 100  $\mu\text{l}$  fresh culture medium containing 10% CTB stock solution was added to each well and the cells were incubated at 37 °C in a 5% CO<sub>2</sub>, 21% O<sub>2</sub>, humidified atmosphere for 1.5 h before measuring the fluorescence signal.

## 2.6. Lactate dehydrogenase based viability assay

Another colorimetric method commonly used to determine cell viability is the evaluation of lactate dehydrogenase (LDH) activity in the cell culture supernatant. Damaged or dead cells with compromised membrane integrity release LDH from the cytosol into the cell culture medium. Here, the Cytotoxicity Detection Kit (Roche, Basel, Switzerland) was used, and a spectrophotometric microplate reader (BioTek Instruments, Inc. Winooski, VT, USA) allowed for simultaneous measurement of multiple samples. The amount of leaked, active LDH is measured by the conversion of tetrazolium salt into the red formazan, which possess an absorption maximum at 500 nm. Therefore, the amount of formazan is directly proportional to the count of damaged cells, and can thus be used to measure cell viability. The LDH assay was performed as instructed by the manual, including controls. Cells were seeded as described in section 2.5 and 100  $\mu\text{l}$  supernatant from each well were used for the calculation of cell viability by LDH assay.

## 2.7. Cell growth on 3D printing material

Cell cultivation chambers were designed via CAD software; 3D-printed; post-processed; disinfected with ethanol (70%, v/v); and then washed thoroughly with sterile PBS for the use in cell culture. Figure 5 illustrates the dimensions and handling of the 3D-printed system. The whole system fits in a well of a regular 6-well plate, which facilitates user-friendly handling without compromising sterility. A cultivation surface for adherent cell growth is placed in a cavity in the middle of the system that is hereafter referred to as the 'cell cultivation well'. The growth surface area of the cell cultivation well is adapted to the growth area of a regular well in a 24-well plate and is 1.89 cm<sup>2</sup>. Therefore, experiments in regular 24-well plates served as a control, an ideal cultivation. However, it should be noted that the regular 24-well plates used are coated with unknown formulations, designed by the manufacturer to provide an optimum culture substrate (Sarstedt AG & Co. KG, Nürnberg, Germany). Accordingly, the 3D-printed system is actually being compared to ideal cultivation conditions.

Before the start of an experiment, the 3D-printed cell cultivation chambers were immersed in ethanol (70%, v/v; 1 h) for disinfection. Afterwards, they were placed in a sterile environment on a sterile surface for at least 30 min allowing residues of ethanol to evaporate. Finally, the 3D-printed systems were washed thoroughly with sterile PBS. Cells were seeded in cell cultivation wells at a density of 15.000 cells · cm<sup>-2</sup>. As control cultures, cells were seeded at the same density in 24-well plates (Sarstedt AG & Co. KG, Nürnberg, Germany), which have the same growth surface area of 1.89 cm<sup>2</sup> as the 3D-printed cultivation wells. All cultures were maintained at 37 °C in a 5% CO<sub>2</sub>, 21% O<sub>2</sub>, humidified atmosphere. After 24 h and 48 h, cell viability was evaluated via a CTB viability assay (see section 2.5). Cell proliferation was also determined via Trypan blue exclusion method. The Trypan blue stain can enter and thereby mark dead or damaged cells, as they possess compromised membrane integrity. On that account, living and dead or damaged cells can be distinguished. Cells were stained with 0.4% Trypan blue stain (n = 3) and living just as dead cells counted in a haemocytometer (Brand GmbH + Co. KG, Wertheim, Germany). In addition, apoptosis and necrosis of cells were analysed by flow cytometry after seeding of cells directly onto 3D-printed material. Figure 1 presents an overview of the conducted method steps for analysing biocompatibility of the 3D-printed material.

## 2.8. Contact angle measurement

The contact angle between water droplets and the 3D-printed material surfaces was determined using a contact angle meter (OCA 50 15EC, DataPhysics Instruments GmbH, Filderstadt, Germany). 1 µl of deionized water was dropped onto the material surface.

The measurement (optical recording by camera) was started immediately and corresponding software (SCA 20, DataPhysics Instruments GmbH, Filderstadt, Germany) was used to estimate the contact angles. All sides of the surface structure formed by the 3D printing process and the surface of a commercial cell culture well plate were analysed. For each material surface five independent measurements were performed.

## 2.9. Cell viability analysis by flow cytometry

Flow cytometry is a technique used to identify cell phenotype and characteristics by using light-scattering properties of cells and their fluorescence activity. Flow cytometry renders it possible to not only differentiate between living and dead cells, but also to draw correlations between cell apoptosis vs. necrosis using specific fluorescence detection markers. Analyses of apoptosis vs. necrosis is particularly useful because it provides a researcher with more detailed information regarding the influences of the 3D printing material on cell behaviour and cell death. Single cells are hydrodynamically focused in a liquid stream, and, as they pass the interrogation point, a light beam of suitable wavelengths is directed to hit single cells—permitting the research to analyse the light scattering effect caused by that cell's physical characteristics.

The BD FACSAria™ Fusion (Becton Dickinson, Franklin Lakes, NJ, USA) flow cytometer was used in this study. Cells were seeded in 3D-printed cultivation chambers or regular 24-well plates, respectively, with a density of 15.000 cells · cm<sup>-2</sup> and incubated at 37 °C in a 5% CO<sub>2</sub>, 21% O<sub>2</sub>, humidified atmosphere. After a defined period of time, cells were detached via accutase treatment, centrifuged for 5 min at 200 xg, and washed with PBS twice. Apoptotic and necrotic cells were then visualized via specific fluorescence staining. An early event happening during apoptosis is the translocation of phosphatidylserine to the cell surface. The detection of these residues on the surface of the cell can therefore be considered to constitute a clear sign of apoptosis. Annexin V has a high binding affinity for phosphatidylserine and therefore can be used as a marker protein for detecting apoptosis. Here, apoptotic cells were identified using a PE Annexin V stain (Becton Dickinson, Franklin Lakes, NJ, USA). The corresponding green fluorescence signal has an excitation maximum of 496 nm, and an emission maximum of 578 nm. Necrotic cells are visually marked using a red fluorescent dead cell stain—here, propidium iodide (Becton Dickinson, Franklin Lakes, NJ, USA). As in the Trypan blue exclusion method, propidium iodide enters cells with disrupted cell membranes, resulting in a fluorescent label of dead cells as a consequence of DNA intercalation. The red fluorescent signal was then measured at an excitation maximum of 493 nm and an emission maximum of 636 nm.

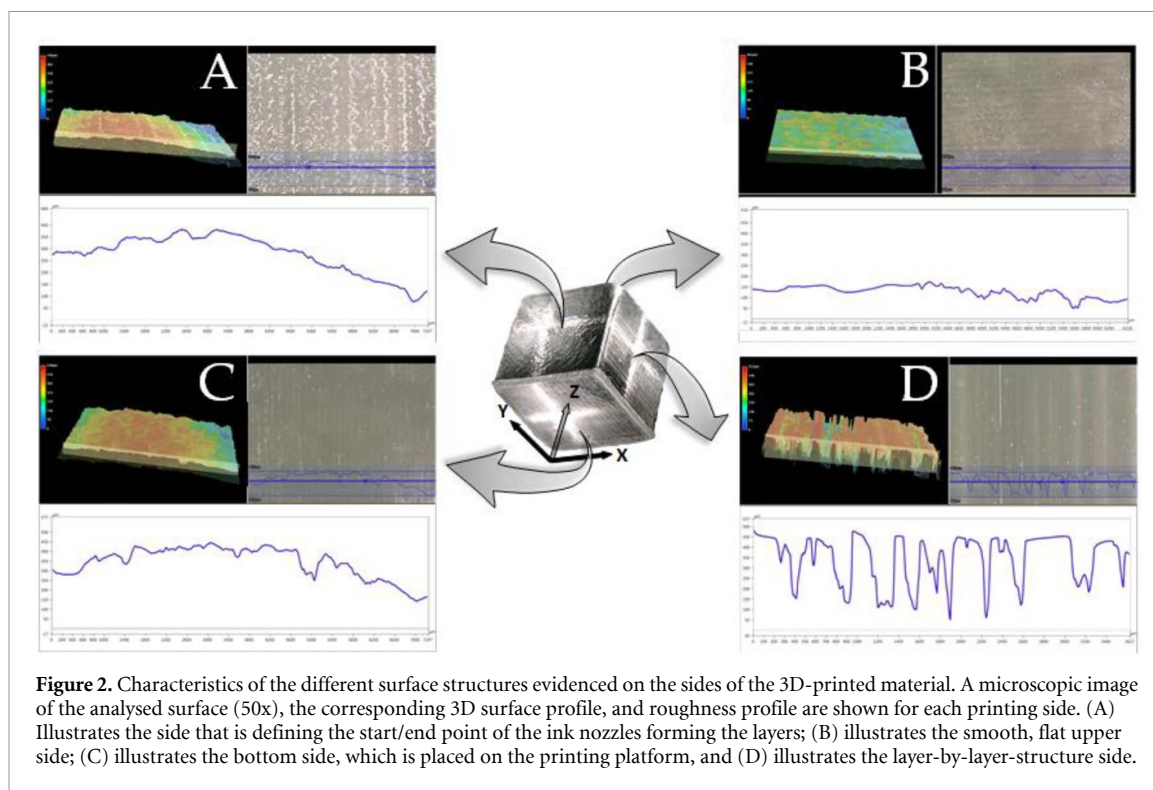


**Figure 2.** Characteristics of the different surface structures evidenced on the sides of the 3D-printed material. A microscopic image of the analysed surface (50x), the corresponding 3D surface profile, and roughness profile are shown for each printing side. (A) Illustrates the side that is defining the start/end point of the ink nozzles forming the layers; (B) illustrates the smooth, flat upper side; (C) illustrates the bottom side, which is placed on the printing platform, and (D) illustrates the layer-by-layer-structure side.

As a negative control, cells were cultivated in original cell culture medium, without any contact to 3D-printed material. For analysing flow cytometry data, the BD FACS Diva™ Software v8.0 (Becton Dickinson, Franklin Lakes, NJ, USA) was used. The basic principle of analysing flow cytometry data is predicated on ‘gating’ cell populations of interests. Cells with common characteristics will appear in one population, and can be analysed and quantified separately from other cells. In this way, living, apoptotic, and necrotic cell populations have been identified. In order to ensure a sufficient sample size to draw accurate conclusions, a uniform gating strategy was maintained and at least 10 000 events per sample were analysed, with an ‘event’ being defined as a single particle being detected.

### 3. Results and discussion

#### 3.1. Analysis of the 3D printing materials’ surface topography

In order to use a material in cell culture applications, the material must not only be sterile and biologically compatible, but it must also have a surface structure and other properties, which are suitable for the intended application. The surface topography and properties of a material can therefore have a high impact on potential applications for that material [19, 20]. For example, an opaque material would not be a good choice for any applications requiring optical analyses. For this reason, the investigation of the surface structures of individual cultivation vessels produced by rapid prototyping is of great importance.

Here, the 3D printing process creates four different surface structures. The specific characteristics of each surface structure with regard to the objective appearance and surface roughness are presented in figure 2. The first surface structure is the bottom side, which is directly placed on the printing platform (see figure 2(C)). The stripes visible in this surface structure are generated by the ink nozzles of the 3D printer, and are therefore entirely dependent on the distance that exists between those nozzles. As shown in the roughness profile of figure 2(C), this first surface exhibits small irregularities in height due to the structure of the printing platform. During forward movement of the printing head, the ink is pushed through the nozzles. A roller sitting right behind the nozzles smooths the printed bands into a flat layer before a UV-lamp cures the ink. The smoothing of the roller creates a flat layer, which constitutes the second surface structure (see figure 2(B)). This upper side always has the flattest surface structure in any object printed using this process. In the further course of the printing process, layer upon layer is stacked to form the desired object. This creates a striped appearance on two sides of the cured material resulting in a third surface structure type—as defined as the layer-by-layer structure side (see figure 2(D)). These structures evidence highest surface roughness. Figure 2(A) represents the fourth formed surface structure, which results from the start and end points of the ink nozzles forming the layers. It also shows a slightly striped appearance generated by the different ink layers.

For applications with direct cell-material interaction, the materials’ surface topography must allow

for cell adhesion and proliferation *without* influencing cell morphology [21]. Distinct irregularities in height of the material's structure can result in accumulations and detachment of cells at specific locations, and thereby cause problematic inhomogeneity of cell growth on the surface [21, 22]. For this reason, the upper material side smoothed by the roller of the 3D printer was chosen for growth experiments with cells. Here, the printing process did not cause any distinct height irregularities, neither in the direction parallel to the printing direction nor at a 90° angle to the printing direction, as the roughness profiles show (see figure S3 in supporting information (available online at [stacks.iop.org/BMM/15/055007/mmedia](https://stacks.iop.org/BMM/15/055007/mmedia))). By regulating the orientation of the intended 3D-printed object before printing, the desired surface structure can be selected for specific object details. In this study, we orientated the CAD model—and thus the resulting 3D-printed system—in order to ensure that the smoothed, uniform surface structure was located at the area where cells would be seeded. In contrast to our application—*e.g.* general cultivation with simultaneous observation of cells growing on 3D printing material—other applications may actually require surfaces with a higher relative degree of roughness, so the extent that an increased adhesion or accumulation of cells and corresponding cellular behaviour could be deemed beneficial in other contexts [23–25].

Furthermore, the physical shape of an object may have a significant impact on a biological application, just as hardness and flexibility are important values that must be taken into account [12]. For all biomedical applications, sterile systems are absolutely mandatory. Previous published work has demonstrated the importance of a suitable sterilization or disinfection procedure for 3D-printed objects used in cell culture applications [26]. Many 3D-printed materials lack a high heat distortion temperature, which forecloses the possibility of using any thermal sterilization techniques (*e.g.* autoclaving) [14, 15]. Because the polyacrylate material used in this study deforms at temperatures around 80 °C, thermal sterilization is not possible. Therefore, a chemical disinfection method using ethanol (70 %, v/v) was used in this study.

However, contact with chemical solvents as ethanol can affect the surface properties of a material. Thus, a surface study using different organic solvents used in conventional laboratory routine was also conducted. Treatment with isopropyl alcohol (70 %) and ethanol (70 %) were shown to have no significant impact on the surface roughness, weight, colour, or overall appearance of the investigated 3D-printed material up to an incubation period of 24 h. The corresponding results can be found in the supporting information in figures S1 and S2. Furthermore, previous work demonstrated the suitability of ethanol as an effective disinfectant without influencing optical or mechanical properties of a 3D-printed material [26].

Many 3D-printed materials also evidence a high water uptake and associated swelling—which can result in deformations of the printed systems, and may have a corresponding impact on durability and strength of the material [12]. Especially for devices where small details are of critical importance (for example, microfluidic channels), deformations should be avoided at all costs since they can render the printed device unfunctional. The 3D-printed material used in this study was particularly developed by the manufacturer (Keyence Deutschland GmbH, Neu-Isenburg, Germany) to minimize water uptake and swelling. Indeed, no water uptake was detected for an incubation period of 14 d in performed weight experiments (figure S2 in supporting information).

### 3.2. Testing the biocompatibility of the 3D printing material in accordance to ISO 10993-12:2012

Whenever foreign material is considered for use in biomedical applications, guaranteed biological compatibility is also an absolute prerequisite. For polymer-based materials, potentially cytotoxic effects on cells can emanate from leaching of remaining acrylate monomers or degradation, and can result in irritations and/or allergic reactions within the human body [12, 27, 28]. The 3D printing material used has not yet been certified as biocompatible, nor has it been introduced to a biological environment with mammalian cells. Therefore, general biocompatibility studies were initially carried out.

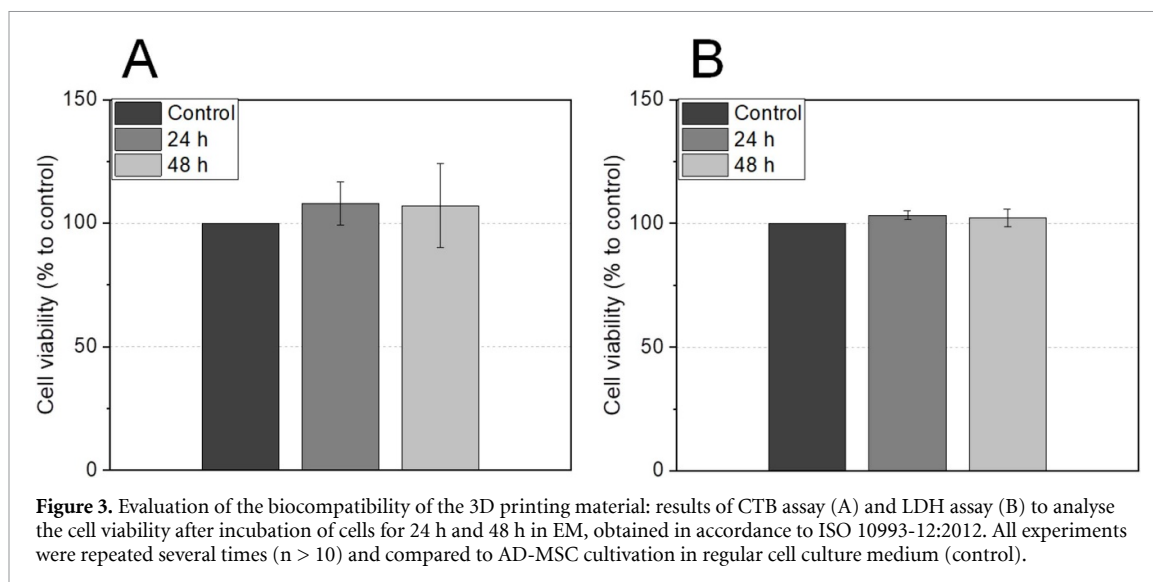
To investigate the potential cytotoxicity of the 3D-printed polyacrylic material, two different *in vitro* viability assays were conducted—each relying on a different process in the cellular metabolism. Both assays are biochemical-based and widely used, providing results that are both reliable and specific in nature [12, 29]. For both the CTB assay and the LDH assay, AD-MSCs were cultivated in EM, which was prepared beforehand according to EN ISO 10993-12 (2012) (see section 2.3). The results of both viability assays are presented in figure 3, in which cell viability is normalised to the control.

Neither assay revealed any significant differences in cell viability when compared with control cultures (cell viabilities of cells incubated in the EM of around 107% in CTB assay and 102% in LDH assay). In summary, then, this EM does not contain any toxic substances leading to negative effects on the cell's viability. Therefore, the analysed 3D printing material can be considered as (*in vitro*) biocompatible according to ISO 10993-12:2012.

### 3.3. Cell growth in 3D-printed cultivation chambers

Depending on the application, biological systems may be in either direct or indirect contact with the material of a cultivation vessel or other equipment. In the case of direct contact, many material's properties can influence the suitability of the material





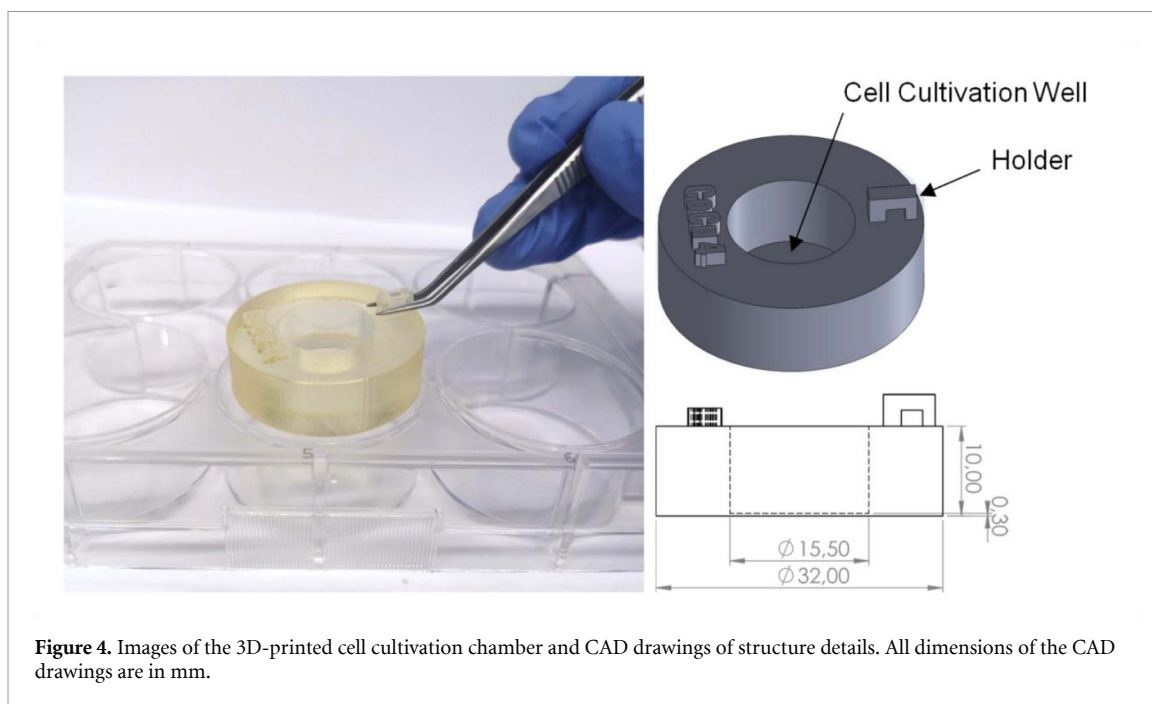
in the desired biological application, since cells are very sensitive to their direct environment [12]. As mentioned above, mechanical and physical properties such as surface roughness, swelling, and wettability can all have a major impact on cell adhesion and proliferation [19, 20]. Optical properties such as transparency and color of the material are also of great importance for microscopic applications. Here, a transparent solid cultivation chamber was 3D-printed. Depending on the thickness of the 3D-printed object, the cured material can take on a slightly yellowish tinge—however, the transparency of the 3D-printed material still allows for direct microscopic monitoring of cell cultures even when this tinge is present. Application fields, that partially require optical monitoring of experiments—such as microfluidics or cell culture technology—can benefit from the material’s optical properties [30].

Figure 4 illustrates a 3D-printed prototype of a cell cultivation chamber. The dimensions of this system are adapted to fit in a well of a regular 6-well plate. By placing the system within a sterile 6-well plate, not only sterile conditions but also a user-friendly handling approach can be achieved. AD-MSCs were seeded in a cavity in the middle of the system—the cell cultivation well—which has a material thickness of 0.3 mm to the bottom. The growth surface area of the cell cultivation well is 1.89 cm<sup>2</sup>, and is designed to match the growth area of regular 24-well plates. Thus, it is possible to perform control cell cultivations in regular 24-well plates with equal growth surface area for comparison. However, it should be noted that control cultivations represent the optimal growth of AD-MSCs as the regular 24-well plates used in this study are coated with an unknown formulation in order to obtain an optimal culture substrate on the part of the manufacturer.

Figure 5 demonstrates representative microscopic images of cells growing directly on 3D-printed

material in the cell cultivation chamber and control cells plated in regular well plates after a cultivation period of 30 h. Microscopic analyses of cell growth, cell morphology, and layer formation showed no differences for AD-MSCs growing on 3D-printed material when compared with control cultures in regular well plates. In addition, contact angle measurements were performed on the different sides of the material surfaces formed by the 3D printing process. The contact angle quantifies the wettability of a surface and can be used as an indicator for cell adhesion [31]. All surfaces analysed, including the control surface of regular cell culture well plates, exhibited comparable water contact angles around 80° (78.41°–83.73°). The comparable contact angles thus indicate similar cell adhesion tendency to the 3D printing material as well as the regular cell culture plates. However, other material properties such as surface charge and energy can also potentially affect cellular adhesion and proliferation.

In addition, the cell growth and viability of AD-MSCs cultured in 3D-printed cultivation chamber was determined by cell counting using Trypan blue staining and CTB assays (see sections 2.7 and 2.5). Results of both analyses are presented in figure 6. Both analyses showed no significant differences—regardless of whether AD-MSCs grew on the 3D-printed material or on the material surface of regular well plates. Up to a cultivation period of 44 h, the number of living cells increased in the average by a factor of 4.5 for control cultivations, and 4.1 for cells growing on 3D-printed material (see figure 6(A)). After 44 h, only minor additional changes in cell growth can be observed (since a cell confluency of 100% has been achieved by that point). Furthermore, viability analyses of cells growing in direct contact to the 3D-printed material showed no significant differences to control cultures—resulting in  $95 \pm 7.4\%$  after a cultivation period of 24 h and



**Figure 4.** Images of the 3D-printed cell cultivation chamber and CAD drawings of structure details. All dimensions of the CAD drawings are in mm.

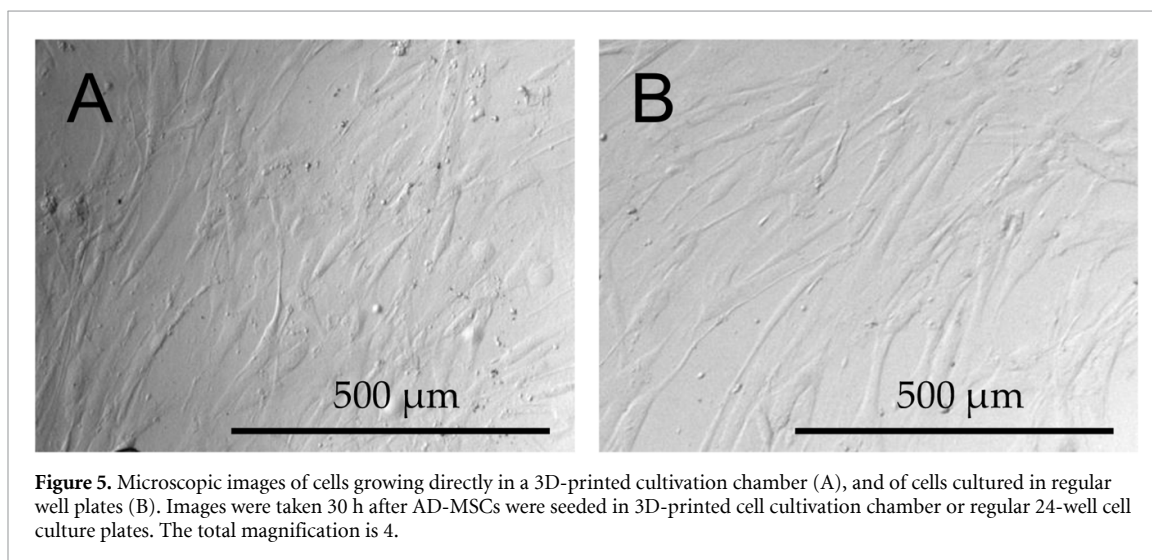


**Figure 5.** Microscopic images of cells growing directly in a 3D-printed cultivation chamber (A), and of cells cultured in regular well plates (B). Images were taken 30 h after AD-MSCs were seeded in 3D-printed cell cultivation chamber or regular 24-well cell culture plates. The total magnification is 4.

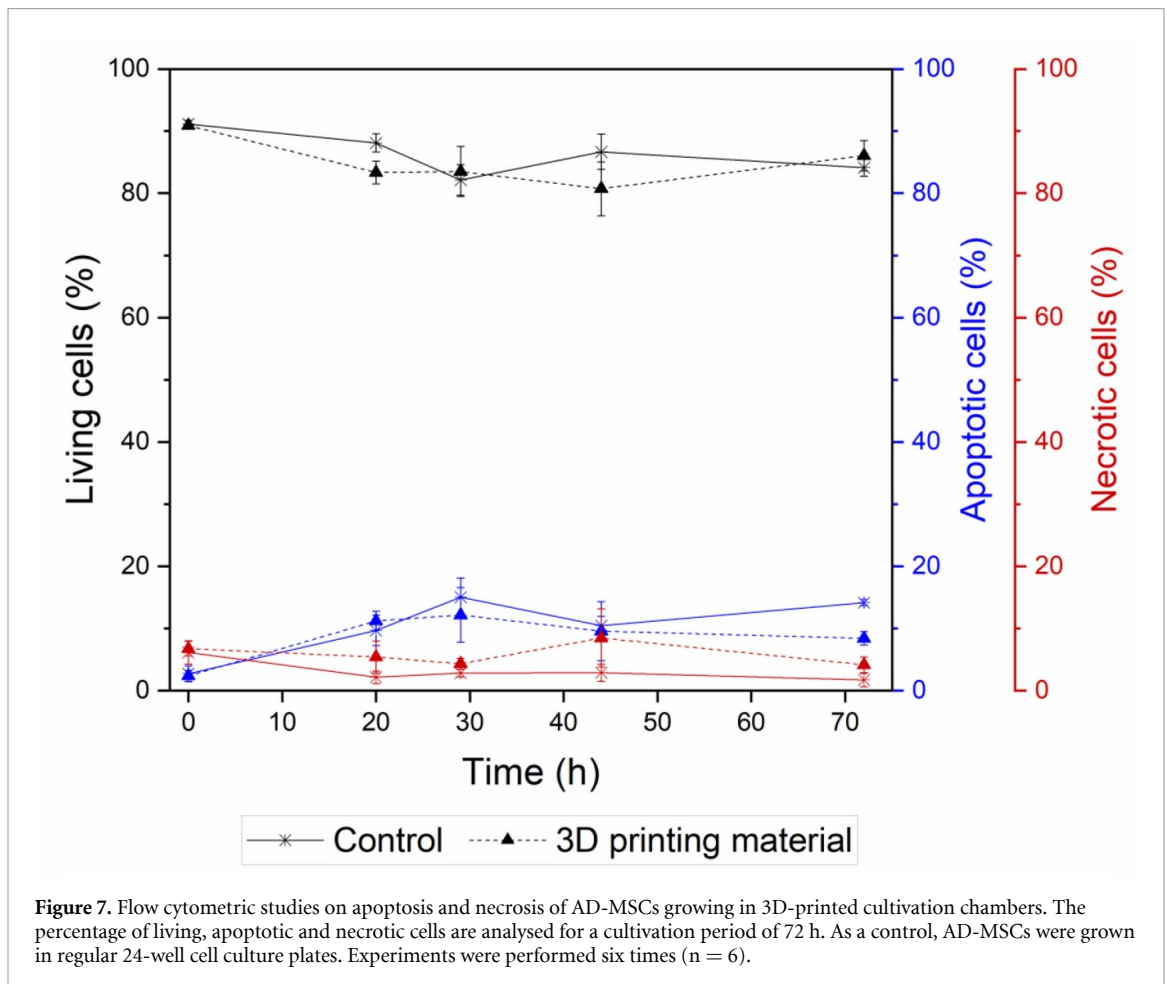
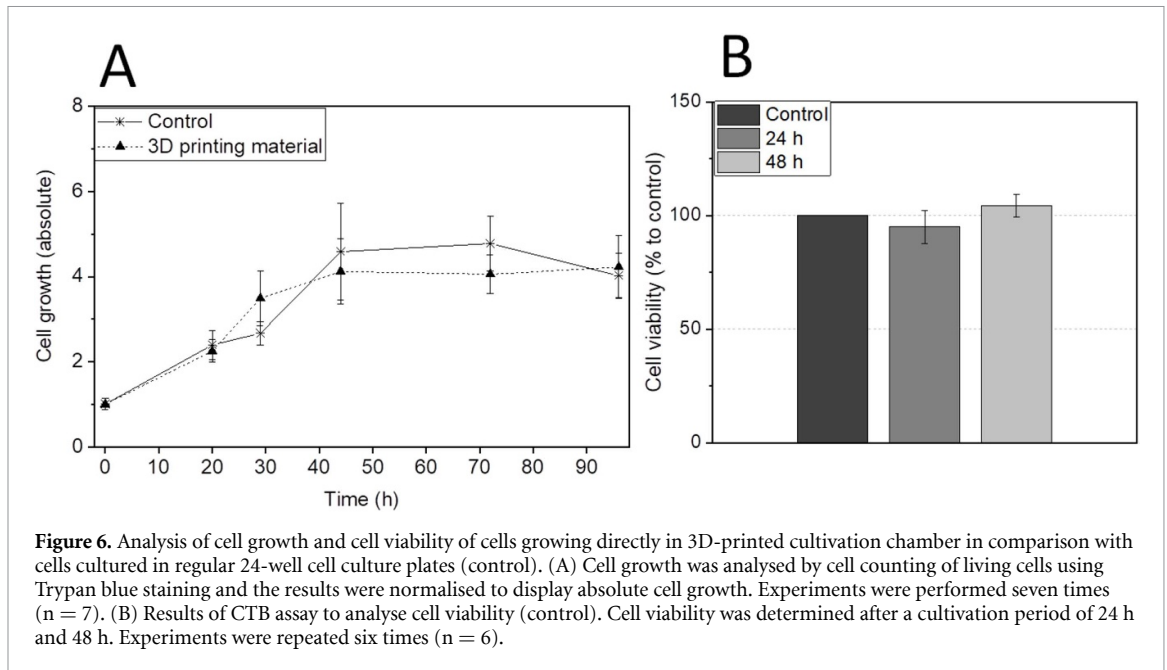
$104.5 \pm 4.95\%$  after 48 h of cultivation on 3D-printed material. In summary, neither cell growth nor cell viability appears to be restricted by this 3D-printed material.

However, CTB assay only allows for conclusions based on the fundamental distinction between living and dead cells—it does not provide any more general information about the different mechanisms by which cell death may occur. Apoptosis and necrosis analyses contain important additional data, which can help a researcher to assess the impact of the 3D-printed material on cell behaviour. As a result, additional apoptosis and necrosis analyses were also conducted via flow cytometry. While apoptosis represents the endogenous mechanism of a regulated or ‘programmed’ cell death, the necrosis pathway is often described as an unregulated form of cell death occurring in response to external stresses

such as physical injuries, chemical substances, or pathogens [32, 33]. Both pathways present divergent morphological and biochemical characteristics, from which specific fluorescent detection markers for flow cytometry analyses can allow conclusions to be drawn.

#### 3.4. Characterization of cell state using flow cytometry

Physical cell characteristics such as size and information about the internal complexity (i.e. granularity), as well as fluorescent signals, can easily be analysed via flow cytometry. By using specific fluorescent markers to detect and differentiate between apoptotic and necrotic cell features, cell death response can be monitored and quantitatively investigated (see section 2.9). Cells undergoing apoptosis can be identified by using a fluorescence annexin V dye, which



is detecting the translocation of phosphatidylserine to the cell surface—a typical attribute of apoptosis [33]. Since necrotic cells possess a compromised cell membrane, specific fluorescence dyes (here propidium iodide) can enter the cell and intercalate in DNA structures [33]. As a result, cells with

disrupted cell membranes can be visually detected and quantified using this method. The relative percentages of living, apoptotic, and necrotic cells—cultured directly in 3D-printed cultivation chambers and in regular well plates as a control—is presented in figure 7.

Across both cultivation systems (i.e. AD-MSCs growing in direct contact to 3D-printed material, and AD-MSCs cultivated on regular well plate surfaces), no obvious difference with respect to the relative percentages of living, apoptotic, and necrotic cells was detected. The relative percentages of living cells decreased for both cultivation systems from about 91% at the beginning of the experiment to percentages ranging between 81% and 86% during the further cultivation process. The relative percentage of apoptotic cells increased from 2.5% at the beginning of the cell cultivations to about 15% after 29 h of cultivation. In the further cultivation process, a decline of 4% in respect to the relative percentage of apoptotic cells cultured 3D-printed cultivation chambers was observed—while control cultures again showed a slight increase of the percentage of apoptotic cells after 72 h. The simultaneous decrease in the count of living cells and increase in the percentage of apoptotic cells at the beginning of the experiment may be related to the adaption of the AD-MSCs to their new environment and cell culture medium. Changes of cell culture medium and environment can be associated with cellular stress, which causes a decrease in cell viability [34, 35]. Except for a point of time of 44 h after AD-MSCs were seeded in the respective cultivation wells, both cultivation systems showed similar courses of the relative percentages of necrotic cells. After a cultivation time of 44 h, AD-MSCs growing in 3D-printed cultivation chambers showed a slightly increased count of necrotic cells but no significant differences to the control cultivation.

In keeping with previous investigations, no significant differences in regard to apoptotic and necrotic cell death responses were observed between cells cultured directly in 3D-printed cell cultivation systems and in regular well cell culture plates. The 3D printing material used here has no negative effect on the AD-MSCs. It is important to mention that the used material has not yet been certified as biocompatible and there have been no publications demonstrating the use of this material for biological applications. Therefore, our results show for the first time that the 3D printing material used here has a high potential for the production and application of customized cell culture vessels and devices.

#### 4. Conclusions

This study not only presents a thorough examination of a not yet certified 3D printing material with regard to surface quality and biocompatibility, but also it shows a comprehensive characterization of a customized 3D-printed cell culture system for potential use in biological applications. Considered collectively, the experiments discussed above demonstrated that this 3D-printed material is suitable for applications requiring either direct or indirect cell contact—which

opens the door for its use in countless applications in the fields of biotechnology and biomedicine. Because no significant differences in cell behaviour and response, morphology, or proliferation could be identified between this material and control cultivations, this material can also be characterized as (*in vitro*) biocompatible. Moreover, the translucent clear appearance of the 3D-printed material enables optical experiments—such as microscopic monitoring of cell cultures, or tracing of liquids within microfluidic applications.

The relevance of the 3D printing material analysed here is indisputable: taking into account both the benefits of 3D printing technology and the outstanding properties of this material, we believe that this study should open the door to a wide range of biological applications going forward—in particular in the field of personalized cell culture technology and 3D cell culture.

#### Acknowledgments

The authors would like to thank Niklas-Maximilian Epping for his support to this work. Also, we acknowledge the corporation with Sarah Strauss and Peter Vogt (Hannover Medical School, Hannover, Germany), who provided tissue material for hAD-MSCs isolation. Furthermore, we would like to thank the group of Oliver Plettenburg (Institute of Organic Chemistry, Hannover, Germany) for providing the live cell imaging microscope and the group of Detlef Bahnemann (Institute of Technical Chemistry, Hannover, Germany) for providing the contact angle meter.

This research was funded by the German Research Foundation (DFG) via the Emmy Noether Programme, project ID 346772917, and the publication of this article was funded by the Open Access fund of Leibniz Universität Hannover.

Author contributions: I G S, A E and J B designed the experiments. I G S conducted the experimental work, drafted and revised the manuscript. P G and S W assisted with cell culture experiments. A L, T S and J B supervised the work, revised the manuscript, and provided helpful ideas for the present work.

#### Ethics approval and consent to participate

The use of donated tissues and cells is approved by the local ethics committee of Hannover Medical School (reference number 3475-2017). Patients gave their written consent for tissue donations. Consents were archived within the patients' charts. All donations were performed anonymously and were not traceable by the scientists. The set of information for the scientists contained only age and gender. Patients with severe co-morbidities were not included in the study at hand.

## Conflicts of interest

The authors declare no conflict of interest.

## ORCID iD

Ina Gerhild Siller  <https://orcid.org/0000-0002-5755-7550>

## References

- [1] Hull C W 2015 *Res.-Technol. Manag.* **58** 25–30
- [2] Jones D B, Sung R, Weinberg C, Korelitz T and Andrews R 2015 *Surg. Innov.* **23** 189–95
- [3] Ventola C L 2014 *Pharm. Ther.* **39** 704–11
- [4] Coakley M and Hurt D E 2016 *J. Lab. Autom.* **21** 489–95
- [5] Raddatz L, Vries I D, Austerjost J, Lavrentieva A, Geier D, Becker T, Beutel S and Scheper T 2017 *Eng. Life Sci.* **17** 931–9
- [6] Enders A, Siller I G, Urmann K, Hoffmann M R and Bahnemann J 2019 *Small* **15** 1804326
- [7] Brimmo A, Goyette P-A, Alnemari R, Gervais T and Qasaimeh M A 2018 *Sci. Rep.* **8** 10995
- [8] Macdonald N P, Cabot J M, Smejkal P, Guijt R M, Paull B and Breadmore M C 2017 *Anal. Chem.* **89** 3858–66
- [9] Papenburg B J, Rodrigues E D, Wessling M and Stamatialis D 2010 *Soft. Matter.* **6** 4377–88
- [10] Yang S Y, Kim E-S, Jeon G, Choi K Y and Kim J K 2013 *Mater. Sci. Eng. C: Mater. Biol. Appl.* **33** 1689–95
- [11] Lourenco B N, Marchioli G, Song W, Reis R L, van Blitterswijk C A, Karperien M, van Apeldoorn A and Mano J F 2012 *Biointerphases* **7** 46
- [12] Bernard M, Jubeli E, Pungente M D and Yagoubi N 2018 *Biomater. Sci.* **6** 2025–53
- [13] Lu Z, Jiang X, Zuo X and Feng L 2016 *RSC Adv.* **6** 102381–8
- [14] 3D Systems I 2016 *Safety Data Sheet: VisiJet EX 200, VisiJet M3 Crystal: According to Regulation (EC) No 1907/2006 and 1272/2008, Hazard Communication Standard 29 CFR 1910 (USA), WHS Regulations Australia, JIS Z 7253 (2012) Japan (3D Systems I)*
- [15] 3D Systems I 2018 *Safety Data Sheet: VisiJet M2R-CL: According to Regulation (EC) No 1907/2006 and 1272/2008, Hazard Communication Standard 29 CFR 1910 (USA), WHS Regulations Australia, JIS Z 7253 (2012) Japan (3D Systems I)*
- [16] Pepelanova I, Kruppa K, Scheper T and Lavrentieva A 2018 *Bioengineering* **5** 55
- [17] O'Brien J, Wilson I, Orton T and Pognan F 2000 *Eur. J. Biochem.* **267** 5421–6
- [18] Niles A L, Moravec R A and Riss T L 2009 *Curr. Chem. Genomics* **3** 33–41
- [19] Thevenot P, Hu W and Tang L 2008 *Curr. Top. Med. Chem.* **8** 270–80
- [20] Wang Y-X, Robertson J L, Spillman W B J R and Claus R O 2004 *Pharm. Res.* **21** 1362–73
- [21] Kocijan A, Conradi M and Hočevar M 2019 *Materials* **12** 1877
- [22] Lampin M, Warocquier-Clérout R, Legris C, Degrange M and Sigot-Luizard M F 1997 *J. Biomed. Mater. Res.* **36** 99–108
- [23] Angelova N and Hunkeler D 1999 *Trends Biotechnol.* **17** 409–21
- [24] Pattanaik B, Pawar S and Pattanaik S 2012 *Indian J. Dent. Res.* **23** 398–406
- [25] van Midwoud P M, Janse A, Merema M T, Groothuis G M M and Verpoorte E 2012 *Anal. Chem.* **84** 3938–44
- [26] Siller I G, Enders A, Steinwedel T, Epping N-M, Kirsch M, Lavrentieva A, Scheper T and Bahnemann J 2019 *Materials* **12** 2125
- [27] Kopperud H M, Kleven I S and Wellendorf H 2011 *Eur. J. Orthod.* **33** 26–31
- [28] Rashid H, Sheikh Z and Vohra F 2015 *Eur. J. Dent.* **9** 614–9
- [29] Eisenbrand G et al 2002 *Food Chem. Toxicol.* **40** 193–236
- [30] Walczak R 2018 *Bull. Pol. Acad. Sci., Tech. Sci.* **66** 179–86
- [31] Dowling D P, Miller I S, Ardhauoui M and Gallagher W M 2011 *J. Biomater. Appl.* **26** 327–47
- [32] Tang D, Kang R, Berghe T V, Vandenaabeele P and Kroemer G 2019 *Cell Res.* **29** 347–64
- [33] Wlodkowic D, Telford W, Skommer J and Darzynkiewicz Z 2011 *Methods Cell Biol.* **103** 55–98
- [34] Garcia-Montero A, Vasseur S, Mallo G V, Soubeyran P, Dagorn J C and Iovanna J L 2001 *Eur. J. Cell Biol.* **80** 720–5
- [35] Young J W, Locke J C W and Elowitz M B 2013 *Proc. Natl. Acad. Sci. USA* **110** 4140–5